Published Online: 26 September, 2011 | Supp Info: http://doi.org/10.1083/jcb.201103117

Transmembrane segments of nascent polytopic membrane proteins control cytosol/ER targeting during membrane integration

Pen-Jen Lin,[1] Candice G. Jongsma,[2] Shuren Liao,[4] and Arthur E. Johnson[1,2,3]

[1]Department of Molecular and Cellular Medicine, Texas A&M Health Science Center, [2]Department of Chemistry, and [3]Department of Biochemistry and Biophysics, Texas A&M University, College Station, TX 77843
[4]Fox Chase Cancer Center, Philadelphia, PA 19111

During cotranslational integration of a eukaryotic multispanning polytopic membrane protein (PMP), its hydrophilic loops are alternately directed to opposite sides of the ER membrane. Exposure of fluorescently labeled nascent PMP to the cytosol or ER lumen was detected by collisional quenching of its fluorescence by iodide ions localized in the cytosol or lumen. PMP loop exposure to the cytosol or lumen was controlled by structural rearrangements in the ribosome, translocon, and associated proteins that occurred soon after a nascent chain transmembrane segment (TMS) entered the ribosomal tunnel. Each successive TMS, although varying in length, sequence, hydrophobicity, and orientation, reversed the structural changes elicited by its predecessor, irrespective of loop size. Fluorescence lifetime data revealed that TMSs occupied a more nonpolar environment than secretory proteins inside the aqueous ribosome tunnel, which suggests that TMS recognition by the ribosome involves hydrophobic interactions. Importantly, the TMS-triggered structural rearrangements that cycle nascent chain exposure between cytosolic and lumenal occur without compromising the permeability barrier of the ER membrane.

Introduction

In eukaryotic cells, most membrane proteins are integrated into the membrane of the ER cotranslationally at sites termed translocons (Johnson and van Waes, 1999; Rapoport, 2007; Skach, 2009). The insertion and correct threading of a polypeptide into a phospholipid bilayer as the nascent protein is being synthesized is a complex operation, especially for multispanning polytopic membrane proteins (PMPs) with hydrophilic segments (loops) that are alternately directed to opposite sides of the membrane. This process is further complicated because an unregulated release of Ca^{2+} ions into the cytosol from their storage location inside the ER would have severe metabolic consequences for the cell. Thus, cotranslational protein integration must be completed with minimal disruption of the membrane permeability barrier.

Various aspects of PMP integration have been examined previously, but three fundamental mechanistic issues have yet to be addressed experimentally: How are the PMP loops alternately directed into the cytosol or ER lumen during translation? What controls the timing of redirecting the PMP nascent chain from one side of the membrane to the other? How does the ribosome–translocon complex (RTC) maintain the permeability barrier of the ER membrane and prevent ion passage through the membrane during PMP integration?

Nascent chain exposure to the cytosol has been examined most frequently by its sensitivity to cleavage by cytosolic proteases. Another approach detects collisions between cytosolic iodide ions and fluorescent dyes incorporated into the nascent chain. Despite the difference in the size of the detectors, proteases versus I^-, both approaches showed that most nascent secretory proteins were not exposed to the cytosol during translocation into the ER lumen (Johnson and van Waes, 1999). In contrast, studies of single-spanning membrane proteins (SSMPs)

P.-J. Lin and C.G. Jongsma contributed equally to this paper.

Correspondence to Arthur E. Johnson: ajohnson@medicine.tamhsc.edu

Abbreviations used in this paper: BiP, binding immunoglobulin protein; εNBD-Lys, Nε-6(7-nitrobenz-2-oxa-1,3-diazol-4-yl)aminohexanoyl-Lys; MLT, melittin; PMP, polytopic membrane protein; pPL, preprolactin; PTC, peptidyl transferase center; RNC, ribosome-nascent chain complex; RTC, ribosome–translocon complex; SSMP, single-spanning membrane protein; TMS, transmembrane segment; VSVG, vesicular stomatitis virus protein G.

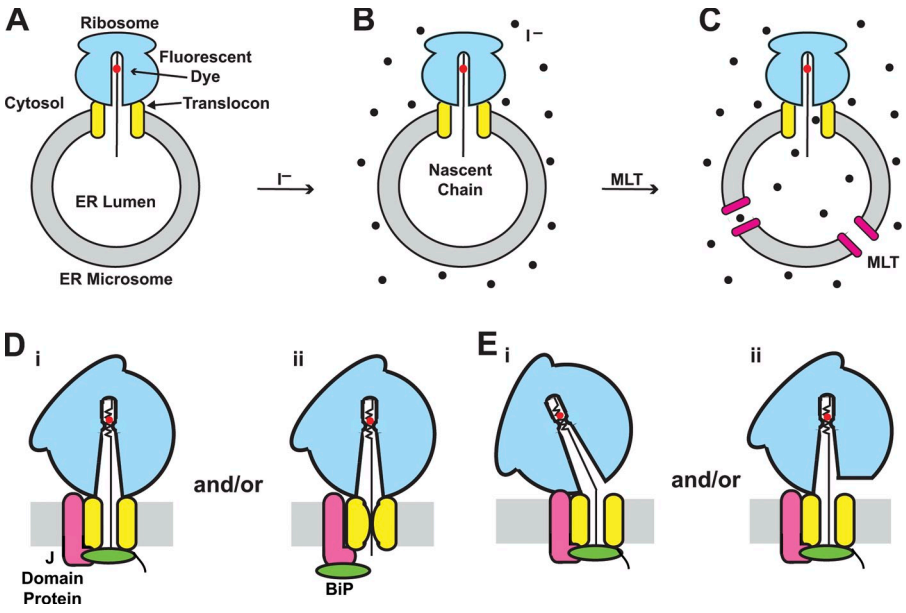

Figure 1. **Nascent chain exposure to cytosol and lumen.** In a quenching experiment, the initial net emission intensity (F_0) of a sample of ER microsome-bound RNCs with an NBD dye (red) located inside the ribosomal tunnel is measured (A) after purification by gel filtration. After addition of KI/KCl (B), the net intensity (F) is measured again to quantify the extent of collisional quenching by cytosolic I^-. MLT is then added to create pores in the ER membrane (C), and the net intensity is remeasured to quantify the extent of quenching by I^- in both cytosol and lumen. (D) Ion flow through the aqueous translocon pore is prevented on the cytosolic side of the membrane by an ion-tight ribosome–translocon junction, and on the lumenal side of the membrane by BiP and a J-domain protein (Alder et al., 2005), acting directly (i) and/or indirectly (ii). (E) Nascent chain exposure to cytosolic I^- may result from conformational changes in the RTC (i) and/or by the dissociation of an RTC-associated protein(s) (ii). Depicted species are not drawn to scale.

using these techniques showed that nascent SSMPs were exposed to the cytosol during their integration, as well as after integration was complete (Liao et al., 1997; Mothes et al., 1997; Cheng and Gilmore, 2006). Furthermore, by examining SSMP accessibility to both lumenal and cytosolic I^-, the nascent chain in the ribosome tunnel was found to be: (a) exposed to the ER lumen and inaccessible from the cytosol, (b) exposed to the cytosol and inaccessible from the ER lumen, or (c) occasionally inaccessible from either side of the membrane (Liao et al., 1997). The key observation was that iodide ions were never allowed to pass freely from one side of the ER membrane to the other during SSMP integration. Thus, the permeability barrier of the membrane was maintained throughout (Liao et al., 1997).

Although the mechanisms that accomplish SSMP biogenesis may also be involved in PMP integration, the periodic redirection of nascent chain from one side of the membrane to the other during PMP integration substantially complicates matters. In particular, mechanisms must exist that dictate when major structural rearrangements occur at and in the membrane to effect an inversion of nascent chain deposition. By directly monitoring the exposure of PMP nascent chains inside the ribosome tunnel to both cytosol and lumen, we have shown here that PMP exposure alternates from one side of the membrane to the other as the nascent chain lengthens. Furthermore, we have correlated each inversion of PMP loop exposure to the entry of a nascent chain transmembrane segment (TMS) into the tunnel (in this paper, "tunnel" refers to ribosome tunnel and "pore" refers to translocon pore). Ribosomes appear to recognize TMSs at a site far inside the tunnel, and each nascent chain TMS in turn, irrespective of loop size, triggers major RTC structural and functional changes upon reaching that tunnel location. The timing of PMP nascent chain loop inversion from cytosolic to lumenal or the reverse during integration is therefore dictated by ribosomal recognition inside the tunnel of each TMS, the structural element in the nascent chain that demarcates successive PMP loops.

Results

Approach

To examine cotranslational PMP integration at a defined point, a truncated mRNA was added to an in vitro translation. Protein synthesis ceased when the ribosome reached the end of the mRNA, thereby creating ribosome-nascent chain complexes (RNCs) with nascent chains of the same length, each attached to a tRNA because the mRNA lacked a stop codon. Successive stages in integration were examined by increasing the length of truncated mRNA and hence nascent chains.

To monitor PMP surroundings and interactions during biogenesis, a fluorescent probe was incorporated into a PMP nascent chain at a specific site using an experimental approach we originated (Johnson et al., 1976). A chemically modified Lys-tRNA, N^{ε}-6(7-nitrobenz-2-oxa-1,3-diazol-4-yl)aminohexanoyl-Lys-$tRNA^{Lys}$ (εNBD-Lys-$tRNA^{Lys}$), was added to an in vitro translation programmed with a truncated mRNA containing only a single Lys codon. The resulting RNCs contained only a single probe, positioned in the nascent chain according to the coding sequence. In this study, probes were usually located in a TMS near the C-terminal end of the nascent chain, far inside the ribosomal tunnel and >50 Å from the exit. TMS hydrophobicity was retained because εNBD-Lys is not charged.

Nascent chain exposure to the cytosol or lumen was detected by the collisional quenching of NBD fluorescence (Crowley et al., 1993; Johnson, 2005). When an I^- collides with an excited NBD dye, the dye loses its excited state energy and returns to the ground state without the emission of a photon, thereby reducing (quenching) the fluorescence of the sample. If the emission intensity of an NBD-containing RTC sample is not quenched by I^- addition, then the NBD dyes are not accessible to I^- in the sample. Such a result would show that there is no aqueous pathway through which a hydrated I^- can diffuse that connects the aqueous ribosome tunnel to an aqueous compartment containing I^-. This straightforward technique detects directly whether a nascent chain NBD is exposed to ions in the

cytosol or lumen, and also whether an ion permeability barrier exists. Because the quenching approach is nondestructive, it is less intrusive than the more commonly used protease accessibility assays that monitor nascent chain cleavage. Collisional quenching also has a higher resolution than other approaches because it uses much smaller probes to detect accessibility (I^- vs. protease).

Compartment-specific quenching is achieved because I^- does not detectably pass through the membrane of purified ER microsomes (Cranney et al., 1983; Crowley et al., 1994). Thus, when I^- is added to a sample of RNC-bound microsomes with their cytoplasmic leaflet on the outer surface (Fig. 1 A), only NBD probes exposed to the cytosol will collide with I^- and be quenched (Fig. 1 B). NBD exposure to the lumen is then given by any additional quenching detected when I^- is introduced into the ER lumen of the same microsomes (Fig. 1 C) by pore-forming proteins (Crowley et al., 1994) or peptides such as melittin (MLT; Alder et al., 2005).

If cytosolic I^- does not quench the emission of nascent chain NBDs located inside the ribosome tunnel, then the RTC must form an ion-tight ribosome–translocon junction that prevents free passage of I^- from the cytosol into the ribosome tunnel (Fig. 1 D). However, if cytosolic I^- quenches NBD emission, then I^- can diffuse into the tunnel though an opening in the junction. We usually depict the loss of a cytosolic ion-tight seal in our cartoons by tilting the ribosomes to indicate a different RTC conformation (Fig. 1 E, i), but the actual structural changes may include the loss and/or rearrangement of RTC-associated proteins that allow I^- access to the ribosome tunnel and hence nascent chain access to the cytosol (Fig. 1 E, ii; Pool, 2009; Erdmann et al., 2011; Devaraneni et al., 2011). I^- does not simultaneously move into the lumen because the other end of the pore is closed to the cytosol by the direct (Fig. 1 D, i) or indirect (Fig. 1 D, ii) action of BiP on the lumenal side of the membrane (Hamman et al., 1998; Haigh and Johnson, 2002; Alder et al., 2005).

After RNC targeting to the translocon by a cleavable signal sequence, the nascent chain is exposed to the lumen but not the cytosol (Crowley et al., 1994). SSMP studies revealed that the appearance of a nascent chain TMS inside the ribosome tunnel triggered structural rearrangements at the ER membrane that reversed nascent chain exposure inside the tunnel from the lumen to the cytosol without compromising the membrane's permeability barrier (Liao et al., 1997; Haigh and Johnson, 2002). Because these very different spectroscopic phenotypes were reproducibly observed in samples that differed only in the length of the nascent chain (Δ = 7 residues), this spectroscopic approach is a sensitive, nondestructive, and high-resolution indicator of nascent chain accessibility and hence the biological state of the sample.

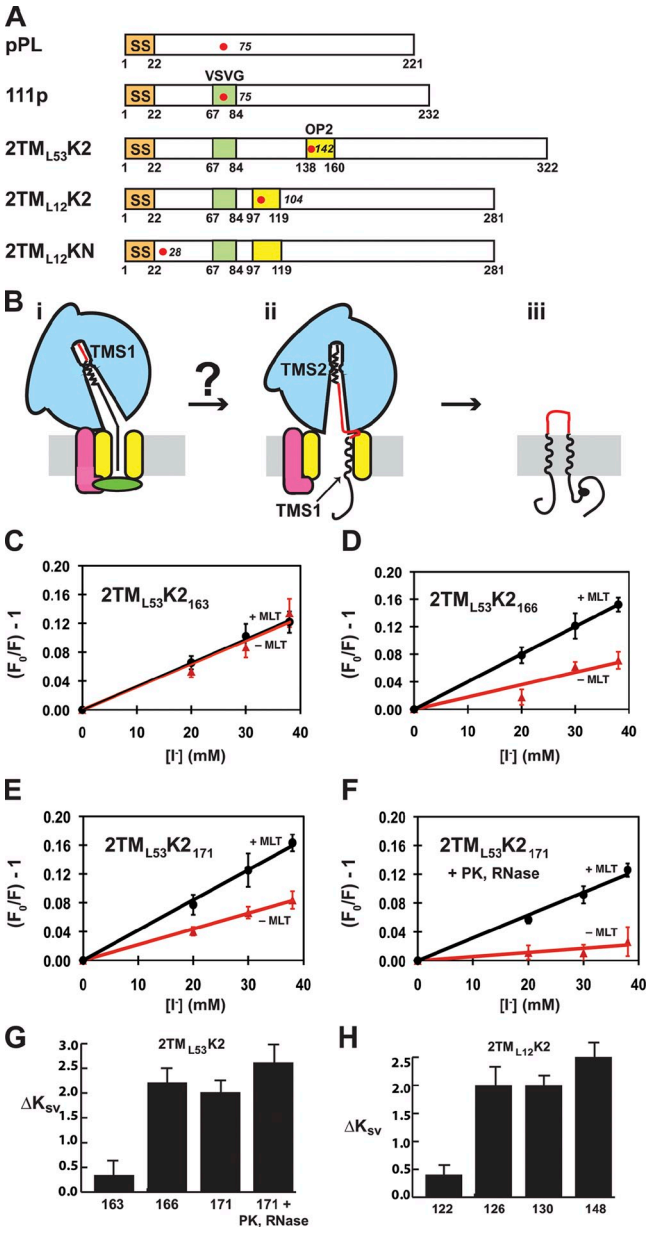

Figure 2. **TMS2 control of RTC structure.** (A) Protein primary structures are depicted to show the locations of topogenic sequences and the single lysine codon (red) in each. TMS1 = VSVG (green); TMS2 = opsin 2 (yellow); SS = pPL signal sequence (orange). (B) The entry of TMS1 into the ribosome tunnel opens the RTC junction and closes the lumenal end of the pore (i). When TMS2 moves into the tunnel (ii), does the RTC junction close and the lumenal end of the pore open? The cytosolic loop sequence after TMS1 is shown in red for the full-length PMP (iii). (C–F) Collisional quenching data for RTCs with the indicated nascent chains obtained before (red ▲) or after (black ●) MLT addition. (G and H) Bar graphs showing the ΔK_{sv} values for the indicated nascent chain lengths of the indicated proteins. Standard deviations and *n* values are shown in Table I. Error bars indicate SD.

TMS2 alters nascent chain exposure

To determine what effect, if any, a second TMS (TMS2) would have on nascent chain exposure, we inserted the second TMS of opsin into the previously characterized 111p SSMP (Fig. 2 A). The resulting nascent PMPs were designated 2TM$_{L53}$K2$_n$ to represent an n-residue nascent protein with two TMSs separated by a loop of 53 residues and a lysine codon-specified probe in TMS2 (K2). Because the residues that follow TMS2 are directed into the lumen instead of the cytosol, the appearance of TMS2 might reverse the changes at the RTC elicited by TMS1 and reestablish an ion-tight RTC junction (Fig. 2 B). I^- accessibility of the TMS2 probe was therefore examined as a function of nascent chain length.

Table I. **Collisional quenching of integration intermediates with two nascent chain TMSs[a]**

PMP[b]	TMS_C-PMP separation[c]	*n*[d]	−MLT K_{sv}[e]	+MLT K_{sv}[e]	ΔK_{sv}
			M^{-1} ± *SD*	M^{-1} ± *SD*	M^{-1}
$2TM_{L53}K2_{163}$	3	4	3.1 ± 0.2	3.4 ± 0.3	0.3 ± 0.4
$2TM_{L53}K2_{166}$	6	3	1.8 ± 0.3	4.0 ± 0.1	2.2 ± 0.3
$2TM_{L53}K2_{171}$	11	6	2.2 ± 0.2	4.2 ± 0.2	2.0 ± 0.3
$2TM_{L53}K2_{171}$ (+PK, RNase)	11	6	0.6 ± 0.4	3.2 ± 0.2	2.6 ± 0.4
$2TM_{L12}K2_{122}$	3	3	2.8 ± 0.1	3.2 ± 0.2	0.4 ± 0.2
$2TM_{L12}K2_{126}$	7	3	2.0 ± 0.2	4.0 ± 0.3	2.0 ± 0.4
$2TM_{L12}K2_{130}$	11	3	1.9 ± 0.1	3.9 ± 0.2	2.0 ± 0.2
$2TM_{L12}K2_{148}$	29	3	1.7 ± 0.1	4.2 ± 0.3	2.5 ± 0.3
$2TM_{L12}KN_{122}$	3	2	2.0 ± 0.5	4.6 ± 0.2	2.6 ± 0.5
$1.5TM_{L53}K1.5_{163}$	15	2	3.4 ± 0.0	3.6 ± 0.1	0.2 ± 0.1
$1.5TM_{L53}K1.5_{171}$	23	2	3.6 ± 0.3	3.8 ± 0.1	0.2 ± 0.3
$2DUP_{L54}K2_{159}$	3	2	4.0 ± 0.2	4.1 ± 0.1	0.1 ± 0.2
$2DUP_{L54}K2_{162}$	6	2	2.0 ± 0.1	4.1 ± 0.1	2.1 ± 0.1
$2INV_{L54}K1_{91}$	3	2	1.1 ± 0.1	3.4 ± 0.4	2.3 ± 0.4
$2INV_{L54}K1_{94}$	6	2	3.1 ± 0.4	3.4 ± 0.1	0.3 ± 0.4
$2INV_{L54}K2_{163}$	3	2	4.0 ± 0.1	4.0 ± 0.1	0.0 ± 0.1
$2INV_{L54}K2_{166}$	6	2	1.9 ± 0.0	4.2 ± 0.2	2.3 ± 0.2

[a]RTC preparation and spectroscopic analyses are described in Materials and methods.

[b]PMP topogenic sequences and NBD locations are shown in Figs. 2 A and 3 G.

[c]TMS_C, C-terminal end of TMS nearest the PTC; TMS_C–PTC separation, nascent chain residues between TMS_C and the PTC.

[d]*n*, number of independent experiments.

[e]–MLT and +MLT, data obtained prior to or after, respectively, melittin addition.

A purified sample of $2TM_{L53}K2_{163}$ integration intermediates was split into four aliquots. Different concentrations of KI were added to each aliquot, along with sufficient KCl to equalize the ionic strength in each. The observed quenching, $(F_0/F) - 1$, was plotted as a function of I^- concentration (Fig. 2 C, red ▲). MLT was then added to each aliquot to introduce I^- into the lumen. Because no increase in quenching was observed (Fig. 2 C, black ●), no NBDs were exposed to lumenal I^-. Instead, all nascent chain NBDs were exposed to the cytosol when the C terminus of TMS2 was located three residues from the ribosome peptidyl transferase center (PTC).

The linear Stern-Volmer plots are characteristic of collisional quenching: doubling $[I^-]$ doubles the number of I^- collisions with the dye and hence doubles the quenching. The slope is equal to K_{sv}, the Stern-Volmer constant, and $K_{sv} = k_q\tau_0$, where k_q is the bimolecular quenching constant and τ_0 is the NBD lifetime in the absence of quencher. Although the collisional frequency between NBDs and I^- in a sample is given by k_q, the K_{sv} values are used here to compare I^- accessibility to NBD for nascent chains of different lengths because the mean NBD fluorescence lifetime, $<\tau_0>$, varied little as TMS2 moved through the ribosome tunnel. The K_{sv} values may differ slightly for NBDs located at different positions within the tunnel because its surface is largely comprised of ribosomal RNA (Armache et al., 2010; Ben-Shem et al., 2010), and variations in the local negative ribosomal RNA charge density (Lu et al., 2007) may cause the local I^- concentration to vary. However, such variations are modulated because of the counterions in the solvent, and we have observed only small variations in K_{sv} values for probes in different locations.

When the slightly longer $2TM_{L53}K2_{166}$ nascent chain was examined, the quenching by cytosolic I^- was less than observed with $2TM_{L53}K2_{163}$ (compare −MLT [▲] in Fig. 2, C and D). Increasing the nascent chain length beyond 166 residues had little further effect, as the K_{sv} values were similar for 166 mer and 171 mer (Table I). Thus, moving TMS2 just three residues further away from the PTC caused a twofold reduction in NBD quenching by cytosolic I^-. This reduction must have resulted from a loss of cytosolic I^- access to nascent chain NBDs because $<\tau_0>$ varies only slightly as a nascent chain is lengthened.

Addition of MLT to the $2TM_{L53}K2_{166}$ samples increased I^- quenching of NBD by approximately twofold (Fig. 2 D, ●). Because this increase resulted from the introduction of I^- into the microsomes, the MLT-dependent quenching (the difference between K_{sv} values observed with and without MLT = ΔK_{sv} = 2.2 M^{-1}) reveals that some NBDs were accessible only to lumenal I^- (NBDs exposed to the cytosol would have been quenched before MLT addition). Thus, some 166-mer NBDs were quenched by lumenal I^- (ΔK_{sv} = 2.2 M^{-1}) and others by cytosolic I^- (−MLT K_{sv} = 1.8 M^{-1}), whereas 163-mer NBDs were quenched only by cytosolic I^- ($\Delta K_{sv} = \sim 0\ M^{-1}$; Table I). The similarity of total cytosolic + lumenal quenching of the 163-mer and 166-mer samples (+MLT K_{sv}; Table I) suggests that the twofold difference in cytosolic quenching (−MLT K_{sv}) occurs because some NBDs accessible to cytosolic I^- in the 163-mer sample become accessible only to lumenal I^- in the 166-mer sample. Such a change in quenching is most likely explained by an RTC structural rearrangement that moves nascent chain NBDs from cytosolic to lumenal exposure.

In previous studies with short nascent secretory and SSMP proteins, quenching heterogeneity was minimal because the NBDs were accessible to either the cytosol (K_{sv} = 2.0 ± 0.3 M^{-1} ± pore-forming protein), the lumen (K_{sv} = 0.2 ± 0.2 M^{-1} before

and 2.0 ± 0.3 M^{-1} after the addition of pore-forming protein), or neither (K_{sv} = 0.1 ± 0.2 M^{-1} ± pore-forming protein; Crowley et al., 1993, 1994; Hamman et al., 1997, 1998; Liao et al., 1997; Haigh and Johnson, 2002; Alder et al., 2005). The NBDs in nascent secretory or SSMP proteins were therefore were exposed either to cytosolic I^- (ΔK_{sv} = ~0 M^{-1}) or lumenal I^- (ΔK_{sv} = ~2 M^{-1}), but not both.

All nascent PMPs examined here also had ΔK_{sv} values of either ~2 M^{-1} or ~0 M^{-1} (Tables I and II). However, PMP samples with lumenally exposed NBDs (ΔK_{sv} = ~2 M^{-1}) were also quenched by cytosolic I^- (−MLT K_{sv} > 1 M^{-1}). The abnormally high cytosolic quenching could be caused by leaky microsomes, but appears to be a consequence of the longer truncated mRNAs and the longer, more nonpolar PMP nascent chains because all other components in the secretory, SSMP, and PMP samples were identical.

In a previous study (Hamman et al., 1997), RTCs with long nascent secretory proteins containing NBDs positioned inside the lumen were found to be quenched by both cytosolic and lumenal I^-. After a limited nuclease and protease digestion, the cytosolic quenching was reduced by 76% without lowering the lumenal quenching. The digestion was therefore presumed to release cytosolically exposed NBDs in polysomal RNCs and/or nascent chains that copurified with the microsomes but were not properly engaged with translocons. When $2TM_{L53}K2_{171}$ samples were treated with a limited nuclease and protease digestion before purification and exposure to I^-, the initial −MLT quenching of NBD by cytosolic I^- (Fig. 2 F) was substantially reduced, whereas the ΔK_{sv} values were similar before and after digestion (Table I). Thus, NBDs exposed to the cytosol were preferentially released by digestion, whereas all or most lumen-accessible NBDs were retained.

The complexity of the integration process with long PMP nascent chains and multiple TMSs makes it difficult to identify the biochemical state of the cytosol-exposed and digestion-sensitive NBDs, but their selective removal suggests that their RNCs differ from the RNCs of lumen-exposed NBDs. The molecular basis for this heterogeneity in PMP RNCs has yet to be determined, but the most likely explanation is that some PMP RNCs are bound to translocons without forming tight junctions. Their probes would then be exposed to I^- in the cytosol, and the putative incomplete RNC–translocon junction presumably makes the RNCs more sensitive to release by nucleases and/or proteases.

The cytosolically exposed NBDs could have been removed by further digestion (Hamman et al., 1997) to obtain homogeneous samples similar to the secretory and SSMP samples. However, we chose to avoid compromising the biochemical integrity of the sample and did no digestions. Instead, because the unusually high cytosolic (−MLT) quenching appears to originate from RNCs that are not completely engaged with translocons for some reason, we treat the –MLT quenching observed in samples with lumenally exposed NBDs (ΔK_{sv} = ~2 M^{-1}) as background and focus on ΔK_{sv} values of ~0 M^{-1} or ~2 M^{-1} to indicate exposure to the cytosol or lumen, respectively, of nascent chain NBD probes in the ribosome tunnels of intact integration intermediates, an approach that is consistent with our earlier studies.

PMP loop size

When the inter-TMS loop was reduced from 53 to 12 residues (Fig. 2 A), probe accessibility was again dependent on the length of the nascent chain. NBD in $2TM_{L12}K2_{122}$ intermediates were all accessible to cytoplasmic I^- because ΔK_{sv} was ~0, whereas NBDs in $2TM_{L12}K2_{126}$ and longer intermediates were exposed to lumenal I^- because ΔK_{sv} was near 2 (Fig. 2 H and Table I). Thus, the aqueous ribosomal tunnel was contiguous with the cytosol when the C-terminal end of TMS2 was three residues from the PTC, but was contiguous with the ER lumen when the TMS2 C-terminus was seven residues from the PTC (Fig. 2 B). Because TMS2 exposure was converted from cytosolic to lumenal when the TMS2-PTC separation reached seven residues for both the 53- and 12-residue loops, the transition in RTC structure is triggered by the synthesis of TMS2 and its movement into the tunnel, not by the length of polypeptide between TMS1 and TMS2 nor the time needed to synthesize that polypeptide. RTC structure is therefore regulated by a nascent chain TMS from inside the ribosome tunnel.

I^- does not pass through the membrane

During SSMP integration, the permeability barrier of the ER membrane was maintained by BiP-mediated blockage of ion passage through the aqueous translocon pore when the ribosome–translocon junction was open and the ribosome tunnel was exposed to the cytosol (Haigh and Johnson, 2002). To detect I^- entry into the lumen during PMP integration, NBD was incorporated near the N terminus of $2TM_{L12}KN_{122}$ nascent chains (Fig. 2 A). When I^- and later MLT were added to these intermediates, the ΔK_{sv} was 2.6 M^{-1} (Table I). Thus, nascent chain NBDs that had entered the lumen were not quenched when the nascent chain length was 122, whereas NBDs still inside the ribosomal tunnel were quenched by cytosolic I^- through an open RTC junction (ΔK_{sv} = ~0 for $2TM_{L12}K2_{122}$; Table I). Because cytosolic I^- could collide with NBD in the ribosomal tunnel, but not with NBD in the lumen, the lumenal end of the translocon pore was closed when its cytosolic end was opened, thereby maintaining the membrane permeability barrier.

TMS3 reverses the effects of TMS2

Because TMS2 entry into the ribosome tunnel triggered the re-establishment of an ion-tight RTC junction and the redirection of newly synthesized nascent chain into the lumen, it is possible that TMS3 entry into the ribosome would have the opposite effect: the closing of the lumenal end of the translocon pore and the opening of the RTC junction to allow the following nascent chain to pass into the cytosol (Fig. 3 A). TMS3 of opsin was therefore inserted into the 2TM coding sequences to yield 3TM PMPs (Fig. 3 B). When $3TM_{L12,18}K3_{159}$ was translated, the NBD in TMS3 was accessible to lumenal I^- (ΔK_{sv} = 2.3 M^{-1}; Table II and Fig. 3, C and E). However, the TMS3 probe was exposed to cytosolic I^- when the nascent chain was three residues longer (ΔK_{sv} ~0; Table II and Fig. 3, D and E). Because the same results were obtained when the TMS2-TMS3 loop was 50 residues longer (Table II and Fig. 3 F), TMS3 movement into the ribosome tunnel triggered an inversion of RTC structure such that the nascent chain in the tunnel went from

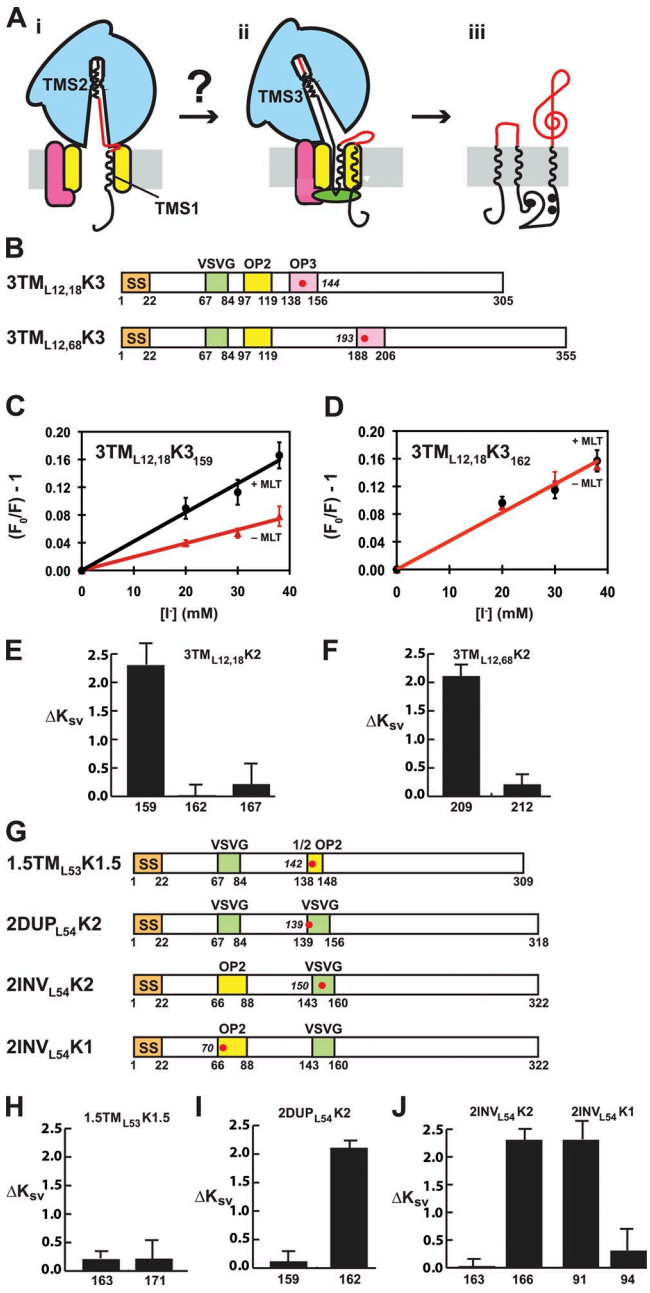

Figure 3. **TMS3 control of RTC structure.** (A) The entry of TMS2 into the ribosome tunnel closes the RTC junction and opens the lumenal end of the pore (i). When TMS3 moves into the tunnel, does the RTC junction open and the lumenal end of the pore close (ii)? The lumenal loop sequence after TMS2 is shown in black, whereas the cytosolic loop sequences after TMS1 and TMS3 are shown in red for the full-length PMP (iii). (B and G) Protein primary structures are depicted to show the locations of topogenic sequences and the single lysine codon (red) in each. TMS3 = opsin 3 (magenta); others are as in Fig. 2 A. (C and D) Collisional quenching data for RTCs with the indicated nascent chains obtained before (red ▲) or after (black ●) MLT addition. The straight lines coincide in D. (E, F, H, I, and J) Bar graphs show the ΔK_{sv} values for the indicated nascent chain lengths of the indicated proteins. Standard deviations and *n* values are shown in Table II. Error bars indicate SD.

lumenal to cytosolic exposure. Because TMS3 reversed the tunnel exposure elicited by TMS2, just as TMS2 reversed the exposure elicited by TMS1, RTC structure appears to alternate between two states in which the aqueous ribosome tunnel is contiguous with either the lumen or the cytosol. Such an arrangement would ensure that newly synthesized hydrophilic loops in a nascent PMP would be alternately directed into the lumen or cytosol. Furthermore, because a TMS in the nascent chain separates successive hydrophilic loops, it is reasonable to control the timing of the two-state RTC transition by a nascent chain TMS.

TMS recognition by ribosomes

Several variations of the 2TM protein were examined to clarify the nature of TMS recognition by ribosomes. When the second half of the TMS2 sequence in the 2TM protein was deleted to yield 1.5TM$_{L53}$K1.5 (Fig. 3 G), the resulting full-length protein was shown by carbonate extraction to be integrated into the bilayer (Fig. 4). However, because the protein was not glycosylated, its C terminus was still in the cytosol. Thus, the 10-residue nonpolar sequence was not recognized as a legitimate TMS by the integration machinery. When examined spectroscopically, a 171-residue nascent chain with the shortened TMS2 did not trigger the closure of the ribosome–translocon junction (Table I; compare Fig. 3 H with Fig. 2 G). Thus, one-half of TMS2 in a nascent chain was not recognized as a TMS, and did not trigger changes at the RTC.

The 2TM and 3TM chimera were constructed so that TMS1 (vesicular stomatitis virus protein G [VSVG], the TMS of the vesicular stomatitis virus G protein), TMS2 (opsin 2), and TMS3 (opsin 3) were each integrated into the ER membrane in their natural orientation (N_{lum} or N_{cyt}). Replacing TMS2 in 2TM$_{L53}$K2 with TMS1 yielded 2DUP$_{L54}$K2, a PMP with a duplicated TMS arrangement (two successive natural N_{lum} TMSs with the same sequence and hydrophobicity; Fig. 3 G). Translation of this protein to full length showed, by carbonate extraction and EndoH treatment, that 2DUP was integrated in the same orientation as the 2TM protein, with both its N and C termini in the lumen (Fig. 5). When nascent chain exposures were compared by I^- quenching, the 2DUP and 2TM proteins looked the same: the ΔK_{sv} was near 0 when the second TMS was three residues from the PTC, and the ΔK_{sv} was near 2 M^{-1} when the TMS2-PTC separation increased to six residues (Table I and Fig. 3 I). Thus, positioning the same N_{lum} TMS twice in succession in the same protein did not affect the TMS-dependent alternation of RTC structure.

The two TMSs in 2TM were then inverted to create 2INV$_{L54}$K, in which the normally N_{cyt} opsin 2 TMS followed the cleaved signal sequence and the normally N_{lum} VSVG TMS replaced TMS2 (Fig. 3 G). Despite this inversion, EndoH treatment and carbonate extraction revealed that the full-length 2INV protein was integrated in the same orientation as the 2TM protein, with both its N and C termini in the lumen (Fig. 5). When examined spectroscopically with a probe in TMS2, 2TM$_{L53}$K2 and 2INV$_{L54}$K2 behaved identically: a ΔK_{sv} near 0 when the second TMS was three residues from the PTC and a ΔK_{sv} near 2 M^{-1} when the TMS2-PTC separation increased to six residues (Table I and Fig. 3 J, left two bars). Furthermore, when the probe was placed in the first TMS of 2INV, its exposure to the cytosol was the opposite of that of TMS2: a ΔK_{sv} near 2 M^{-1} when the first TMS was three residues from

Table II. **Collisional quenching of integration intermediates with three nascent chain TMSs**[a]

PMP[b]	TMS_C-PMP separation[c]	*n*[d]	−MLT K_{sv}[e]	+MLT K_{sv}[e]	ΔK_{sv}
			M^{-1} ± *SD*	M^{-1} ± *SD*	M^{-1}
$3TM_{L12,18}K3_{159}$	3	4	1.9 ± 0.2	4.2 ± 0.3	2.3 ± 0.4
$3TM_{L12,18}K3_{162}$	6	3	4.1 ± 0.2	4.1 ± 0.1	0.0 ± 0.2
$3TM_{L12,18}K3_{167}$	11	3	4.2 ± 0.3	4.4 ± 0.2	0.2 ± 0.4
$3TM_{L12,68}K3_{209}$	3	3	2.0 ± 0.2	4.1 ± 0.1	2.1 ± 0.2
$3TM_{L12,68}K3_{212}$	6	3	3.9 ± 0.1	4.1 ± 0.2	0.2 ± 0.2

[a]RTC preparation and spectroscopic analyses are described in Materials and methods.
[b]PMP topogenic sequences and NBD locations are shown in Fig. 3 B.
[c]TMS_C, C-terminal end of TMS nearest the PTC; TMS_C–PTC separation, nascent chain residues between TMS_C and the PTC.
[d]*n*, number of independent experiments.
[e]−MLT and +MLT, data obtained prior to or after, respectively, melittin addition.

the PTC and a ΔK_{sv} near 0 when the TMS1-PTC separation increased to six residues (Table I and Fig. 3 J, right two bars), which is consistent with earlier SSMP results (Liao et al., 1997). Thus, each TMS of sufficient length, in turn, initiates changes in the RTC structure that alternate between sealing the lumenal or cytosolic end of the translocon pore to direct the nascent chain to the proper compartment.

TMS environment inside the ribosome tunnel is partially hydrophobic

NBD fluorescence lifetime (τ) is very sensitive to its environment (Johnson, 2005): a short 1–2 ns in aqueous solution, but 7–8 ns in the nonpolar core of a membrane (Crowley et al., 1993, 1994). When RTCs were analyzed by time-resolved fluorescence techniques, two discrete fluorescence lifetimes (1–2 and 8–9 ns) were observed in the samples. NBD is therefore found in two different microenvironments within an RTC tunnel, and the mean NBD lifetime, $<\tau>$, reflects the dynamic distribution of NBD between aqueous and nonpolar milieus (Table III).

When NBD was incorporated into nascent preprolactin (pPL) and positioned in the ribosome tunnel 15 residues from the PTC, its 1.5 ns $<\tau>$ was equivalent to that of free εNBD-Lys in aqueous solution (Tables III and IV). Thus, nascent secretory proteins are in a largely aqueous milieu as they pass through the ribosome tunnel, as shown previously (Crowley et al., 1993, 1994). In contrast, when NBD in the middle of an SSMP TMS was positioned 15 residues from the PTC, the molar fraction of NBDs with long lifetimes (f_2) increased dramatically. As a result, the $<\tau>$ for TMS probes was threefold higher than that of pPL probes (Table III). Moving TMS1 into the translocon (probe to PTC = 55 residues) did not significantly alter its NBD lifetime, so the microenvironments for TMS NBDs were very similar inside the ribosome tunnel and translocon pore. The $<\tau>$ inside the tunnel increased slightly when NBD was positioned in TMS2 instead of TMS1, and the TMS2 $<\tau>$ also did not change as the probe moved through the tunnel and into the translocon pore (Table III). Thus, the fluorescence lifetime data, both $<\tau>$ and f_2, reveal that the NBDs in both PMP and SSMP TMSs were in largely nonpolar milieus within the ribosome tunnel and translocon, whereas the NBDs in secretory proteins were surrounded by water.

There are only two options for providing the nonpolar environments detected by the TMS NBDs: the ribosome and the nascent chain itself. To assess their contributions, $2TM_{L12}K2_{126}$ RNCs with NBD in the middle of TMS2 (position 110 instead of 104) were prepared and treated with puromycin to release the nascent chains. Ribosomes were then dismantled by EDTA and RNase A, and the resulting free nascent chains had an NBD $<\tau>$ of 3.6 ns (Table IV). Because this $<\tau>$ was much higher than that of nascent pPL (Table III), the nascent chain contributed significantly to the hydrophobicity of NBD environment, presumably by transient NBD

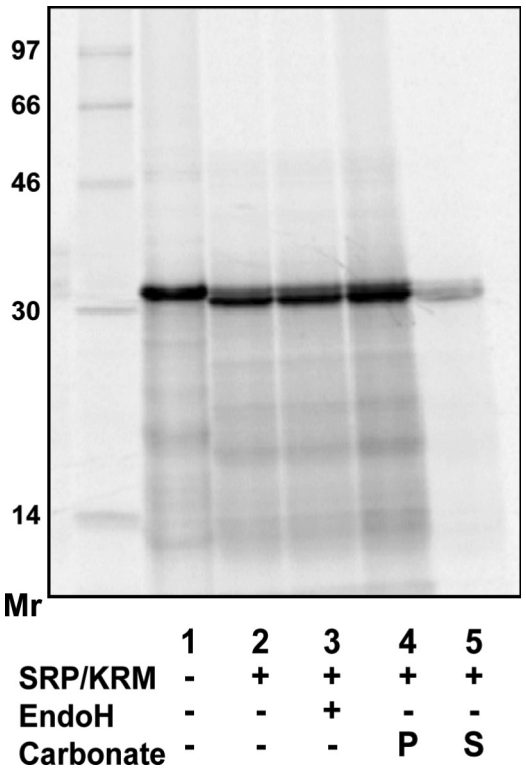

Figure 4. **One-half of TMS2 did not integrate.** Full-length $2INV_{L53}K1.5$ was translated in the presence of ER microsomes, SRP, and [^{35}S]Met, then analyzed by SDS-PAGE. The insolubility in pH 11.5 carbonate shows that the proteins are integrated. Their orientation is N_{lum}-C_{cyt} because the signal sequence is cleaved, but the absence of higher-mass EndoH-sensitive bands shows that the three glycosylation sites in the C-terminal domain are not glycosylated and hence are in the cytosol.

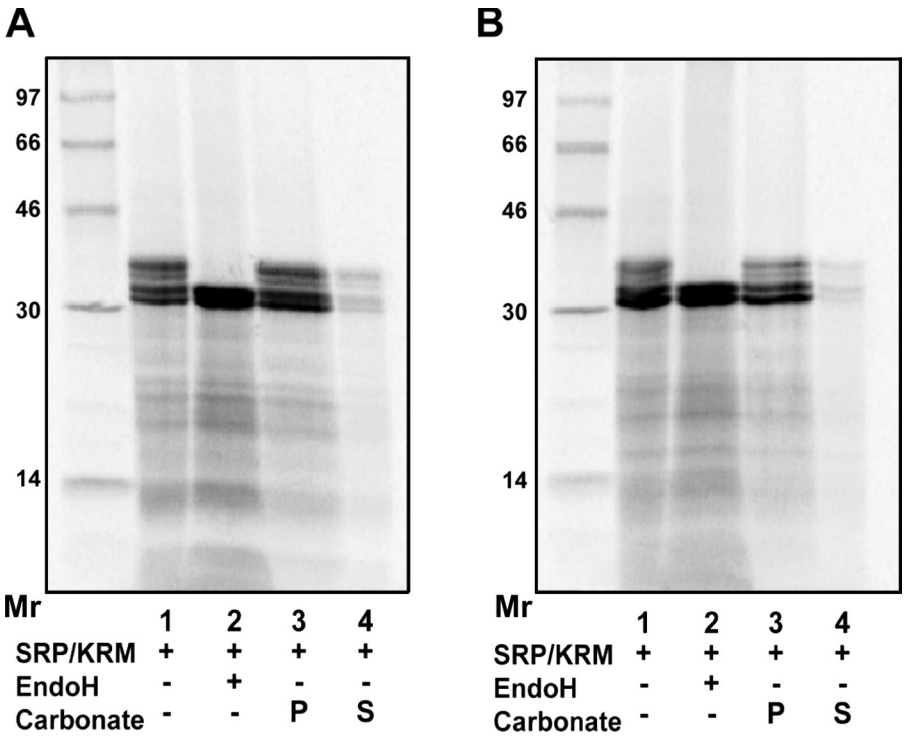

Figure 5. **Integration of 2TM variants.** Full-length $2INV_{L64}K2$ (A) and $2DUP_{L64}K2$ (B) were translated in the presence of ER microsomes, SRP, and [^{35}S]Met, then analyzed by SDS-PAGE. The insolubility in pH 11.5 carbonate shows that the proteins are integrated. The sensitivity of higher-mass bands to EndoH shows that the C-terminal domain was glycosylated and hence in the lumen.

interactions with nearby nonpolar residues and peptide bonds in the TMS. Yet the ribosome also contributed to the nonpolarity detected by NBD because intact $2TM_{L12}K2_{126}$ RTCs had an <τ> of 5.6 ns (Table IV). The longer <τ> of RTCs compared to isolated nascent chains can only be explained by the TMS NBD interacting with nonpolar surfaces on the ribosome tunnel wall. The ribosome dependence of TMS1 and TMS2 environments was also shown by the decrease in <τ> when NBD-TMSs in long nascent chains exited the ribosome tunnel in the absence of membranes and entered the solvent (Table III).

After translation and integration into the ER membrane, full-length $2TM_{L12}K2$ had an NBD <τ> of 6.7 ns (Table IV). This value agrees with the 6–8 ns lifetimes observed for NBDs facing the nonpolar core of the bilayer after membrane insertion of perfringolysin O, a β-barrel pore-forming toxin (Shepard et al., 1998; Shatursky et al., 1999).

Discussion

The sequential insertion of successive TMSs into the lipid bilayer during cotranslational PMP integration has been characterized previously (Sadlish et al., 2005), but the mechanics and timing of directing PMP loops to opposite sides of the ER membrane have not been addressed previously. Here we have examined nascent chain exposure to the cytosol and lumen by a direct and straightforward technique, the collisional quenching of a fluorescent probe incorporated into the nascent chain and

Table III. **NBD fluorescence lifetimes of free and membrane-bound RNCs**[a]

NBD-labeled species[b]	Membranes	Probe-PTC separation[c]	NBD location	τ_1	f_1[d]	τ_2	f_2[d]	χ^2	<τ>[e]
				ns		*ns*			*ns*
pPL_{90}	+	15	Tunnel	0.7 ± 0.1	0.90	8.8 ± 0.2	0.10	4	1.5 ± 0.1
$111p_{90}$	+	15	Tunnel	2.1 ± 0.2	0.61	8.6 ± 0.2	0.39	2	4.6 ± 0.2
$111p_{130}$	+	55	Translocon	2.3 ± 0.4	0.61	7.9 ± 0.5	0.39	1	4.5 ± 0.4
$111p_{130}$	–	55	Solvent	0.8 ± 0.1	0.75	9.2 ± 0.1	0.25	4	2.9 ± 0.1
$2TM_{L12}K2_{122}$	+	18	Tunnel	2.5 ± 0.6	0.50	7.8 ± 0.3	0.50	3	5.2 ± 0.5
$2TM_{L12}K2_{130}$	+	26	Tunnel	2.8 ± 0.1	0.61	9.4 ± 0.1	0.39	7	5.4 ± 0.1
$2TM_{L12}K2_{148}$	+	44	Translocon	2.6 ± 0.2	0.55	9.5 ± 0.2	0.45	3	5.7 ± 0.2
$2TM_{L12}K2_{160}$	+	56	Translocon	2.4 ± 0.3	0.54	9.3 ± 0.3	0.46	4	5.6 ± 0.3
$2TM_{L12}K2_{180}$	–	76	Solvent	1.3 ± 0.3	0.65	8.0 ± 0.3	0.35	1	3.6 ± 0.3

[a]For each RTC, data from three or more independent experiments were combined and analyzed together as described in Materials and methods.

[b]NBD is located at residue 104 of $2TM_{L12}K2$ in these experiments.

[c]Nascent chain residues between nascent chain εNBD-Lys and the PTC.

[d]Molar fraction.

[e]Average lifetime from molar fractions.

Table IV. **NBD fluorescence lifetimes in various environments[a]**

NBD-labeled species[b]	Membranes	Probe-PTC separation[c]	NBD location	τ_1	f_1[d]	τ_2	f_2[d]	χ^2	<τ>[e]
				ns		*ns*			*ns*
εNBD-Lys[f]	–	–	Solvent	1.2 ± 0.2	0.91	2.8 ± 0.2	0.09	1	1.3 ± 0.2
$2TM_{L12}K2_{126}$[g]	–	–	Solvent	2.0 ± 0.1	0.78	8.8 ± 0.3	0.22	3	3.5 ± 0.2
$2TM_{L12}K2_{126}$	–	20	Tunnel	2.2 ± 0.3	0.52	8.6 ± 0.2	0.48	3	5.3 ± 0.3
$2TM_{L12}K2_{126}$	+	20	Tunnel	1.9 ± 0.3	0.49	8.6 ± 0.2	0.51	6	5.3 ± 0.3
$2TM_{L12}K2_{281}$[h]	+	–	Bilayer	2.8 ± 0.5	0.35	10.0 ± 0.3	0.65	1	7.5 ± 0.4

[a]For each RTC, data from three or more independent experiments were combined and analyzed together as described in Materials and methods.

[b]NBD is located at residue 108 of $2TM_{L12}K2$ in these experiments.

[c]Probe–PTC separation, nascent chain residues between nascent chain εNBD-Lys and the PTC.

[d]Molar fraction.

[e]Average lifetime based on molar fractions.

[f]This RTC sample was treated with puromycin, EDTA, and RNase to release the nascent chain from the ribosome into the solvent, and then with proteinase K to digest the nascent chains.

[g]This RTC sample was treated with puromycin, EDTA, and RNase to release the nascent chain from the ribosome into the solvent.

[h]Full-length $2TM_{L12}K2$ proteins were translated and integrated into the ER membrane. The TMS2 and its NBD probe were located in the nonpolar core of the bilayer after their release from the translocon.

located well inside the ribosome tunnel. By monitoring the extent and nascent chain dependence of NBD quenching by I^-, we were able to identify whether the nascent chain in the ribosome tunnel was accessible to cytosolic I^- or to lumenal I^-, as well as determine at what point during translation the nascent chain was exposed to a particular compartment.

Several mechanistic conclusions can be drawn from the data: (a) PMP loop segments are accessible from the lumen or cytosol during integration, and hence are not completely sequestered within the RTC machinery; (b) the nascent chain inside the ribosomal tunnel is exposed to the cytosol or the lumen, but not to both compartments simultaneously; (c) each TMS reverses the RTC structural changes of its TMS predecessor, thereby establishing an obligatory pattern of alternating nascent chain exposure to the cytosol or lumen, and hence loop destination; (d) the timing of structural changes in the RTC that control loop exposure is regulated by nascent chain TMSs; (e) each newly synthesized TMS, regardless of its location in the nascent chain, triggers a change in nascent chain exposure and deposition; (f) a RTC transition is initiated when the C-terminal end of a new TMS moves 6–7 nascent chain residues from the PTC; (g) TMSs are recognized by ribosomes at or near the same location within the tunnel; and (h) ribosomes recognize each TMS inside the tunnel, despite variations in TMS hydrophobicities, sequences, charged residues, natural bilayer orientations, and lengths above an unknown minimum (>10 residues).

These mechanisms ensure that the hydrophilic loops that follow each TMS in the signal-cleaved nascent chain are directed alternately and obligatorily to opposite sides of the ER membrane during PMP integration because each TMS reverses its predecessor's structural changes at the membrane (Fig. 6). Furthermore, because each loop in a PMP is defined by the TMSs at its ends, it is reasonable that each nascent chain TMS triggers a conversion from lumenal to cytosolic pore closure or vice versa. It remains to be seen to what extent these mechanisms are altered, other than their timing, when the first TMS also acts as a signal-anchor sequence (Devaraneni et al., 2011) or when the TMS and/or flanking sequences are ambiguous (Alder and Johnson, 2004; Skach, 2009).

The iodide ion quenching technique also provides a direct approach for assessing whether ions (specifically I^-) pass freely through the membrane and/or RTC, and hence whether a permeability barrier exists at the membrane. Because integration intermediates that differ by only three residues in the length of the nascent chain have stable, reproducible, and dramatically different ΔK_{sv} values (0 vs. 2 M^{-1}; Tables I and II), it is clear that I^- does not pass freely through the ER membrane or RTC because $[I^-]$ would then be the same on both sides of the membrane, and ΔK_{sv} would always be 0 M^{-1}. In those samples with probes that are quenched only by lumenal I^- ($\Delta K_{sv} = \sim 2\ M^{-1}$), quenching of NBDs in the ribosome tunnel by cytosolic I^- must be prevented by a ribosome–translocon junction that provides an "ion-tight" seal (Fig. 6 i). But in samples with $\Delta K_{sv} = \sim 0\ M^{-1}$, the RTC junction is disrupted by conformational and/or compositional changes that expose the nascent chain to the cytosol (Fig. 1 E). Thus, once targeting is complete, each PMP TMS that enters the ribosome tunnel elicits changes in and on both sides of the membrane that expose the nascent chain to the cytosol or lumen, but not to both. Calcium pumps presumably recover any Ca^{2+} leakage that does occur.

Because cryo-EM images show a "gap" of 12–20 Å between the RNC and translocon (Ménétret et al., 2000; Rapoport, 2007), it was proposed that ion flow through the translocon was prevented by a constriction in the pore that only allowed nascent chains to pass (Van den Berg et al., 2004; Rapoport, 2007). Although this model may be operational during nonmammalian posttranslational translocation, key features of this model—the translocon constriction and the absence of an ion-tight RTC junction—are not supported by cotranslational fluorescence quenching data obtained with mammalian translocons. If the ion-tight RTC junction did not exist, the ΔK_{sv} should always be $\sim 0\ M^{-1}$ because cytosolic I^- ($\sim$10 Å hydrated diameter)

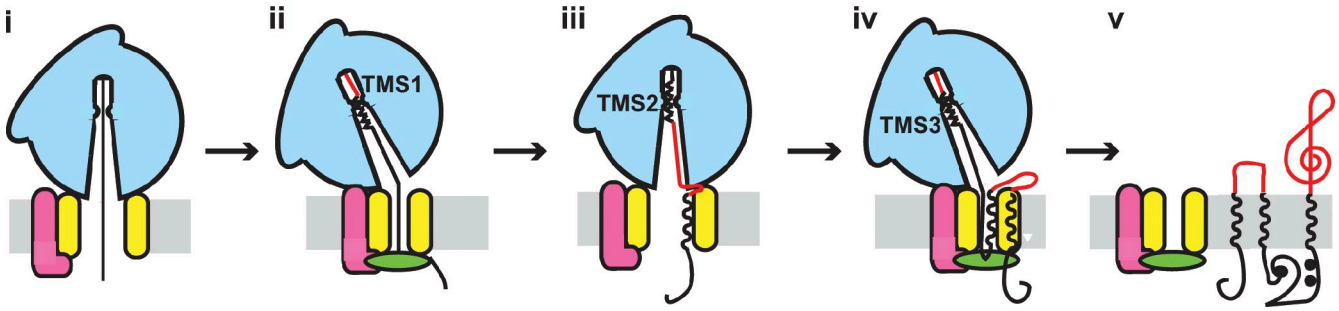

Figure 6. **Cotranslational PMP integration.** After RNC targeting to a translocon, a nascent signal-cleaved PMP in the aqueous ribosomal tunnel and translocon pore is sealed off from the cytosol by an ion-tight junction between the ribosome and translocon/membrane (i). The synthesis and entry of TMS1 into the tunnel triggers BiP-mediated closure of the lumenal end of the pore and the opening of the RTC junction (ii), thereby making the nascent chain inside the tunnel accessible to cytosolic but not lumenal I^-. The entry of TMS2 into the ribosome tunnel reverses the RTC conformational and/or compositional changes elicited by TMS1. Hence, the tight RTC junction is reestablished and the lumenal end of the pore is opened (iii), thereby exposing the nascent chain inside the tunnel to lumenal but not cytosolic I^-. The appearance of TMS3 in the tunnel reverses the changes elicited by TMS2, and the nascent chain in the tunnel becomes accessible to cytosolic but not lumenal I^- (iv). The lumenal loop sequence following TMS2 is shown in black, whereas the cytosolic loop sequences following TMS1 and TMS3 are shown in red for the full-length PMP (v).

would have access to the nascent chain and ribosomal tunnel at all times through the gap. However, nascent chain probes inside the ribosomal tunnel in secretory and some integration intermediates are not accessible to I^- in the cytosol ($\Delta K_{sv} = \sim 2\ M^{-1}$; Tables I and II). Moreover, in samples with a ΔK_{sv} of 2 M^{-1}, I^- and even NAD^+ (Hamman et al., 1997) quench nascent chain NBDs inside the ribosome tunnel, but only after pore formation by MLT allows the quenchers to enter the microsomes (Tables I and II). The quenchers must then move from the lumenal side of the membrane into the ribosomal tunnel through a translocon pore that is already occupied by a nascent chain. Thus, for secretory proteins and some integration intermediates, no constriction is evident that prevents ion movement through the pore of a mammalian translocon bound to a translating eukaryotic ribosome. A large and/or flexible mammalian translocon pore was also indicated by the simultaneous and functional occupancy of an RTC by multiple strands of a nascent PMP (Kida et al., 2007).

The different models for maintaining a permeability barrier during integration result largely from sample differences. Each fluorescence sample contains functional RNCs bound to fully assembled mammalian translocons in native membranes in an aqueous medium, and the presence of intact translocons and membranes ensures that the RTCs maintain the structural arrangement that corresponds to a particular nascent chain–dependent functional state. In contrast, because samples with intact ER membranes cannot be examined by high-resolution cryo-EM images or crystallography, RTCs are prepared with translocon components extracted from the membrane with detergent. The detergent treatment removes lipids, as well as the mammalian translocon core protein translocating chain-associated membrane protein (TRAM) and all or most copies of other translocon-associated proteins (e.g., oligosaccharyltransferase, signal peptidase, TRAP, and SRP receptor; Görlich et al., 1992), thereby altering the composition, conformation, and functionality of the original RTC sample. Hence, the cryo-EM "gap" may result simply because the proteins responsible for filling the gap, perhaps dynamically, do not survive detergent extraction (compare with Fig. 1 E, ii). Consistent with this possibility, nascent chains in membrane-bound RNCs were exposed to the cytosol in the absence of TRAM (Hegde et al., 1998) and calmodulin may have a similar role (Erdmann et al., 2011). In addition, protease digestion at certain stages of integration exposes a nascent chain that is otherwise protected from chemical modification and I^- quenching, thereby demonstrating the protein dependence of the tight ribosome–translocon junction (Devaraneni et al., 2011). Also, because the RNC–translocon junction opens naturally during translational pausing (Hegde and Lingappa, 1996) and protein integration (Liao et al., 1997; Cheng and Gilmore, 2006; this paper), it is possible that detergent-extracted RTCs preferentially adopt an open conformation during cryo-EM sample preparation. Further experimentation will be required to clarify and reconcile the very different views of maintaining the permeability barrier.

Because TMSs in PMPs vary substantially in length, sequence, hydrophobicity, and the presence of charged residues, identifying exactly what structural features are recognized inside the tunnel would require a systematic study beyond the scope of this paper. However, the current data do provide some insights. First, the primary structural feature recognized by the ribosome is a stretch of nonpolar residues in the nascent chain because only TMSs, not the largely hydrophilic sequences in secretory and membrane proteins, elicit changes at the RTC (Tables I and II; Liao et al., 1997). Second, no specific TMS length is required because the VSVG, opsin 2, and opsin 3 TMSs are 18–23 residues in length, and each triggered changes at the RTC (Fig. S1 and Tables I and II). However, 10 nonpolar residues in succession were not sufficient (Fig. 3 G and Table I; Liao et al., 1997). Third, no conserved sequence elements are apparent in TMS1, TMS2, or TMS3 (Fig. S1), which suggests that the RTC changes are not triggered by a specific sequence. Fourth, the hydrophobicities of the VSVG, opsin 2, and opsin 3 TMSs are very different, with whole residue transfer free energies of bilayer insertion (ΔG_{woct}) of −14.6, −6.5, and −5.4 kcal/mole, respectively (White and Wimley, 1999). Yet each TMS triggered changes in the RTC. Notably, the first 10 residues of the VSVG TMS have a total ΔG_{woct} of −7.6 kcal/mole, greater than either TMS2 or TMS3, yet the half TMS was not

recognized by the ribosome as a legitimate TMS. Thus, although some minimum hydrophobicity must be required for a nascent chain sequence to be recognized as a TMS by the ribosome, the spatial extent of nonpolar contact between nascent chain and tunnel surfaces may be a more important criterion. Fifth, the VSVG TMS lacks a charged residue, whereas the opsin 2 and opsin 3 TMSs each have one charged residue (Fig. S1). Thus, a single charged residue in the TMS does not block its recognition by the ribosome. Sixth, the native orientation of a TMS in the bilayer is not recognized by the ribosome because exchanging a native N_{cyt} TMS for a native N_{lum} TMS or vice versa in the nascent chain had no effect on the occurrence or timing of TMS-dependent RTC changes (Table I). Ribosome recognition of TMSs in the tunnel is therefore flexible within limits.

The very different NBD fluorescence lifetimes of nascent membrane and secretory proteins reveal that they are, on average, in different environments within the ribosome tunnel. Secretory proteins are mostly in an aqueous milieu, whereas the TMSs of PMP and SSMP nascent chains are largely in hydrophobic environments (Table III). The nonpolar residues in the TMS near the NBD contribute to its nonpolar environment (Table IV), but the substantial decrease in $<\tau>$ when PMP and SSMP TMSs leave the ribosome tunnel in the absence of membranes suggests that the tunnel surface has nonpolar regions that are accessed by TMSs, but not secretory proteins (Tables III and IV).

The ribosome dependence of TMS NBD $<\tau>$ is most likely caused by the fact that ribosomes must directly contact a nascent chain to identify whether a TMS is present. Given the nonpolarity of TMSs and the great variation in their sequences, a TMS–ribosome interaction is likely to be mediated primarily by hydrophobic association, the major driving force for binding nonpolar entities in an aqueous milieu. This in turn would require the existence of sites on the tunnel wall with nonpolar properties. Because no such sites were evident in the archaeal 50S crystal structure (Nissen et al., 2000), it seems likely that conformational differences, either dynamic or static, between translating ribosomes and the crystal structure are responsible for creating or exposing sites with nonpolar character on the tunnel surface. Such a ligand-dependent conformational change in the tunnel has been observed with a ribosomal protein (Berisio et al., 2003). The number, hydrophobicity, and expanse of such sites on the tunnel surface need not be large, as any TMS–tunnel association must be weak and reversible to ensure that TMSs pass through the tunnel during translation. If this speculation is correct, TMSs in PMP and SSMP nascent chains would partition dynamically between the tunnel surface and the aqueous medium of the tunnel, and transient TMS association with putative nonpolar recognition sites on the tunnel wall would increase the number of NBDs in a hydrophobic milieu, thereby explaining the increased $<\tau>$ and f_2. The dynamics of PMP nascent chain conformation and location within the tunnel is discussed further in the accompanying paper that characterizes TMS folding and movement inside the ribosome tunnel (see Lin et al. in this issue).

Thus, our data indicate that compartment-specific loop deposition and maintenance of the membrane permeability barrier are structurally coupled during cotranslational PMP integration by a complex coordinated choreography of protein–protein and protein–membrane interactions that involve, at a minimum, the nascent chain, the ribosome, the translocon, BiP (Haigh and Johnson, 2002), a J domain–containing membrane protein (Alder et al., 2005), RAMP4 (Pool, 2009), calmodulin (Erdmann et al., 2011), importin α-16 (Saksena et al., 2006), and perhaps others acting in concert as a functional unit (Johnson, 2009). Each TMS that enters the ribosome tunnel triggers an inversion of the operational mode of this coupled functional unit to direct the subsequent PMP loop in the nascent chain into either the lumen or the cytosol. The functional state of this complex is therefore regulated by nascent chain–ribosome interactions from far inside the ribosomal tunnel. The mechanisms that initiate and transmit the signals >100 Å from the TMS in the ribosome tunnel to the ER lumen and the need for early TMS recognition by the RNC are also addressed in an accompanying paper (Lin et al., 2011).

Materials and methods

Plasmids, mRNA, and tRNA

Using standard techniques, PMP plasmids were constructed from lysine-free bovine pPL (each Lys in PL was converted to Q by site-directed mutagenesis) and lysine-free coding sequences within the genes for VSVG, bovine opsin (OP; a gift from R. Gilmore, University of Massachusetts Medical School, Worcester, MA), yeast invertase 2, and human Bcl-2. A single codon in each PMP was then changed to lysine using QuikChange (Agilent Technologies) to position the fluorescent probe at the desired unique site. To avoid ambiguity in interpreting RTC structural changes during integration, fusion proteins were designed with a cleavable signal sequence sufficiently far from the first TMS that RNC targeting to the translocon would be completed before the entire TMS was synthesized. The N-terminus of each membrane protein in this study was therefore comprised of the first 63 residues of pPL modified to remove the lysines in its signal sequence (Crowley et al., 1994; Woolhead et al., 2004). When translated, full-length 111p SSMP contained, from N to C terminus, the pPL fragment, VSVG TMS, invertase 2 (residues 96–130), Bcl-2 (residues 82–141 and 153–182), and lysine-free linkers (Johnson et al., 1995; Do et al., 1996). Full-length $2TM_{L12}$ contained the pPL fragment, VSVG TMS, a 12-residue hydrophilic linker, OP2 TMS, opsin (residues 97–116, the loop following OP2), invertase 2 (residues 96–130), Bcl-2 (residues 92–182), and lysine-free linkers. $2TM_{L53}$ differed from $2TM_{L12}$ only in the loop, where a pPL segment (residues 49–96 with the two K's mutated to Q's) and linker residues replaced the 12-residue loop. Full-length $3TM_{L12,18}$ contained the pPL fragment, VSVG TMS, a 12-residue hydrophilic linker, opsin (residues 74–133 contain the OP2 TMS, the natural intervening loop, and the OP3 TMS), invertase 2 (residues 96–130), Bcl-2 (residues 92–182), and lysine-free linkers. $3TM_{L12,68}$ was created by inserting 40 residues of lysine-free pPL (51–90) and 10 residues of invertase 2 (116–125) after the rhodopsin TMS2-3 loop sequence. The invertase 2 sequence contained three N-linked glycosylation sites that served as marker for whether that polypeptide segment was lumenal (glycosylated) or cytosolic (not glycosylated). Primary sequences were confirmed by DNA sequencing. Truncated mRNAs were transcribed in vitro using SP6 polymerase and PCR-produced DNA fragments of the desired length. εNBD-Lys-$tRNA^{Lys}$ and unmodified yeast Lys-$tRNA^{Lys}$, prepared and purified as described previously (Johnson et al., 1976; Crowley et al., 1993), were obtained from tRNA Probes, LLC.

Integration intermediates

In vitro translations (500 µl) contained: 20 mM Hepes, pH 7.5; 3.0–3.5 mM (optimal concentration was determined experimentally for each lot and a combination of macromolecular components) $Mg(OAc)_2$; 100–130 mM (optimized) KOAc, pH 7.5; 1 mM DTT; 0.2 mM spermidine; 8 µM S-adenosyl-methionine; 1× protease inhibitors (Erickson and Blobel, 1983); 0.2 U/µl RNasin (Promega); 40 µl of an energy-generating system containing 375 µM of each of the 20 amino acids except lysine, 120 mM creatine phosphate, and 0.12 U/µl creatine phosphokinase; 60–80 µl (optimized)

wheat germ extract (Erickson and Blobel, 1983); 40 µl mRNA; 300 pmol of εNBD-Lys-tRNA^{Lys} or Lys-tRNA^{Lys} (tRNA Probes, LLC); and, where indicated, 40 nM purified canine SRP and 80 eq's of canine salt-washed ER rough microsomes (tRNA Probes, LLC). Before the addition of mRNA and tRNA, each sample was incubated at 26°C for 7 min to complete the translation of any residual endogenous mRNA fragments. After mRNA and tRNA addition, reactions were incubated at 26°C for another 40 min. When working with longer nascent chain lengths (171 amino acid residues and longer), the εNBD-Lys-tRNA^{Lys} or Lys-tRNA^{Lys} was added 5 min after the beginning of translation to reduce aa-tRNA deacylation before incorporation.

Two samples were always prepared in parallel, one containing εNBD-Lys-tRNA^{Lys} (the sample) and one containing Lys-tRNA^{Lys} (the blank) to correct for light scattering and background signal. RNCs were purified to remove unincorporated NBD by a high-salt wash and then gel filtration. At the end of a translation, each sample was adjusted to 500 mM in KOAc and incubated on ice for 10 min. Each sample was then loaded onto a separate gel filtration column (Sepharose CL-2B, 0.7 cm inner diameter × 50 cm; column resin must be replaced every 3–4 runs to avoid sample contamination by materials that adsorb to the resin) that had been pre-equilibrated in buffer A (50 mM Hepes, pH 7.5, 40 mM KOAc, pH 7.5, and 5 mM $Mg(OAc)_2$) and then preloaded with 2 ml of buffer B (20 mM Hepes, pH 7.5, 500 mM KOAc, pH 7.5, and 3.2 mM $Mg(OAc)_2$; Haigh and Johnson, 2002). After chromatography at a very slow rate (2–3 drops/min; 4°C) to ensure dissociation of noncovalently bound NBDs, the membrane-bound RNCs eluted in the void volume, typically in 1.1 ml (two 550 µl fractions). Free RNC samples lacking microsomes were treated the same way, except that Sepharose CL-6B was used as the column resin.

More than 50% of the εNBD-Lys-tRNA^{Lys} added to a wheat germ translation of pPL incorporated its amino acid into protein (Crowley et al., 1993). However, in the PMP fluorescence studies, only ∼2% of the εNBD-Lys added to the translation was recovered in the void-volume gel filtration fractions that contained the 2TM and 3TM nascent chains in microsome-bound RTCs due to a combination of effects: losses during purification, less efficient translation of the PMPs than of pPL, and increased losses due to εNBD-Lys-tRNA^{Lys} deacylation when probes were incorporated late in the nascent chain sequence. The final NBD concentration was 5–6 nM in the samples analyzed spectroscopically.

In some cases, samples were exposed to nucleases and proteases for a limited time before gel filtration (Hamman et al., 1997). At the conclusion of the translation, samples received 100 units of *Staphylococcus aureus* nuclease and were made 1 mM in $CaCl_2$ before a 10 min, 26°C incubation. Proteinase K was then added (20 µg/ml translation) and incubated at 0°C for 20 min. PMSF was added to 1 mM and incubated for another 20 min at 0°C to eliminate proteinase K activity. Nucleases and proteases were then separated from the RNCs by gel filtration (see two paragraphs above).

MLT treatment

The honey bee toxin MLT (Sigma-Aldrich; lots from other suppliers varied in activity) was used to induce pore formation in the ER membrane. Lyophilized material could be stored indefinitely, but water solutions of MLT lost their activity after 1 mo and were discarded. MLT was resuspended using ddH_2O, tested for activity, divided into 50 µl aliquots (enough for one quenching experiment), and stored at −80°C. To create pores in the microsomes, MLT was added to each sample to a final concentration of 5 µM, mixed thoroughly (no vortexing), and incubated for 30 min at room temperature in the dark before being re-equilibrated at 4°C in the spectrofluorimeter and remeasured for emission intensity. The addition of MLT to the samples had no effect on targeting, translocation, or signal peptidase activity, nor did it affect the spectral properties of fluorescent translocation intermediates (Alder et al., 2005).

Steady-state spectral measurements

Steady-state data were obtained in buffer A (50 mM Hepes, pH 7.5, 40 mM KOAc, pH 7.5, and 5 mM $Mg(OAc)_2$) on an SLM-8100 photon-counting spectrofluorimeter (SLM) with a 450W xenon lamp, two excitation monochromators, one emission monochromator, and a cooled low-background photomulitplier tube (R928; Hamamatsu) as described previously (Crowley et al., 1993). Samples were maintained at 4°C while nitrogen was flushed through the sample compartment to prevent condensation from forming on the 4 × 4 mm quartz microcuvettes. After additions to a sample, the solution was mixed thoroughly with a 2 × 2 mm magnetic stirring bar as described previously (Dell et al., 1990). Samples were then placed in the sample chamber for 5 min and allowed to equilibrate to 4°C before any measurements were made. To obtain an emission intensity measurement, five successive 5-s integrations of emission intensity were recorded and averaged.

After gel filtration, the light scattering signals of parallel samples were measured (λ_{ex} = 468 nm, λ_{em} = 485 nm) and equalized by diluting the blank or sample as necessary before initiating spectral measurements. Four aliquots (250 µl) of the blank and the sample were then placed in separate microcuvettes (B_0–B_3 and S_0–S_3), and the emission intensity (λ_{ex} = 468 nm, λ_{em} = 530 nm; 4 nm bandpass) was measured for each cuvette. To eliminate any signal caused by light scattering and contaminants, the intensity of a blank was subtracted from the intensity of its cognate sample ($F_{S1} - F_{B1}$, etc.) to yield the net NBD emission intensity for a blank-sample pair. These initial net intensities were later used to normalize the net intensities determined after (KI + KCl) addition.

A 10 µl aliquot containing 1 M KCl was added to B_0 and S_0, whereas the other pairs of cuvettes received varying concentrations of KI:B_1 and S_1, 0.67 M KCl + 0.33 M KI; B_2 and S_2, 0.33 M KCl + 0.67 M KI; and B_3 and S_3, 1 M KI. Each of these aliquots also contained 2 mM $Na_2S_2O_3$, a reducing agent that minimizes I^- oxidation to I_2. The final [I^-] then varied from 0 mM to 38 mM. Higher I^- concentrations were not used because I^- is chaotropic, and RNCs begin dissociating from microsomes when the [I^-] exceeds 70 mM (Crowley et al., 1993). After thorough mixing and temperature re-equilibration, the intensities were remeasured, the blank intensities were subtracted from the cognate sample intensities to yield the net intensities, and then the final –MLT net intensities (F_0, F_1, etc.) were determined by correcting for dilution and using the initial net intensities to normalize the samples to the same initial intensity value (F_0).

After MLT was added to create pores in the ER microsomes and allow free ion passage into and out of the lumen, the blank and sample intensities were measured a third time, corrected for dilution, and normalized to yield the final +MLT net intensities (F_0, F_1, etc.). At the completion of the spectral measurements, samples were analyzed to assess the biochemical state of the εNBD-[^{14}C]Lys in the sample as described previously (Crowley et al., 1993).

Collisional quenching data were analyzed using the Stern-Volmer equation: $(F_0/F) - 1 = K_{sv}[Q]$, where F_0 is the net emission intensity in the absence of Q (here I^-), [Q] is the concentration of quencher, F is the net emission intensity when the quencher concentration is [Q], and K_{sv} is the Stern-Volmer constant. Because the extent of quenching is dependent on the number of NBD collisions with I^-, and hence is directly proportional to [I^-], a linear dependence of quenching [$(F_0/F) - 1$] on [I^-] indicates that the observed quenching is collisional in nature. K_{sv}, the slope of the line, was then determined separately for the +MLT and −MLT data by linear least-squares best-fit graphical analysis in which the line was constrained to go through the origin (0, 0).

Time-resolved spectral measurements

Fluorescence lifetimes were measured in buffer A at 4°C with an ISS K2-002 spectrofluorimeter with a laser diode (λ_{ex} = 470 nm) for excitation. The sample chamber was maintained at 4°C and flushed with N_2 to prevent condensation. NBD emission was collected using a 495 nm cut-on filter, and NBD τ was measured in the frequency domain (2−54 MHz) against a fluorescein (F-1300 [Invitrogen]) dissolved in 0.1 M NaOH) reference (τ = 4.05 ns). The concentration of fluorescein was adjusted to have an emission intensity similar to that of the biochemical samples being examined. The background phase and modulation data from a sample lacking NBD were subtracted from the corresponding data of an equivalent sample containing NBD that was prepared in parallel (Reinhart et al., 1991). Background-subtracted data from three or more independent experiments were combined and fit to several different models to determine which model provided the simplest fit while still yielding a low χ^2 value using Vinci multidimensional fluorescence spectroscopy analysis software (ISS). The best fit was almost always obtained by assuming two discrete exponential decay components. The fit of the data were not significantly improved by assuming the samples contained three components with distinguishable lifetimes, nor by using a Lorentzian fit instead of a discrete fit. The molar fraction of dyes with τ_n is given by f_n, from which the mean lifetime, $\langle\tau\rangle$, was calculated.

To examine the ribosome dependency of the observed lifetime, the NBD τ was measured for free $2TM_{L12}DA2_{128}$ RNCs (Table IV). The free RNCs were then treated with 2 mM puromycin (37°C, 30 min), followed by 5 mM EDTA, pH 7.5, and 20 µg/ml RNase A (final concentrations) at 37°C for 30 min to release the nascent chains from ribosomes. Some samples were also treated with proteinase K (0.1 mg/ml; 30 min; 37°C) to digest the nascent chains and release free εNBD-Lys.

Online supplemental material

Fig. S1 shows the VSVG, OP2, and OP3 TMS sequences, and the probe locations within the TMSs. Online supplemental material is available at http://www.jcb.org/cgi/content/full/jcb.201103117/DC1.

We thank Yuanlong Shao and Yiwei Miao for technical assistance, Reid Gilmore for the opsin plasmid, and Greg Reinhart, J. Martin Scholtz, and C. Nick Pace for advice.

Support was provided by National Institutes of Health grant GM26494, National Science Foundation grant EF-0623664, and Robert A. Welch Foundation Chair grant BE-0017. A.E. Johnson is a founder of tRNA Probes, LLC.

Submitted: 22 March 2011
Accepted: 25 August 2011

References

Alder, N.N., and A.E. Johnson. 2004. Cotranslational membrane protein biogenesis at the endoplasmic reticulum. *J. Biol. Chem.* 279:22787–22790. http://dx.doi.org/10.1074/jbc.R400002200

Alder, N.N., Y. Shen, J.L. Brodsky, L.M. Hendershot, and A.E. Johnson. 2005. The molecular mechanisms underlying BiP-mediated gating of the Sec61 translocon of the endoplasmic reticulum. *J. Cell Biol.* 168:389–399. http://dx.doi.org/10.1083/jcb.200409174

Armache, J.-P., A. Jarasch, A.M. Anger, E. Villa, T. Becker, S. Bhushan, F. Jossinet, M. Habeck, G. Dindar, S. Franckenberg, et al. 2010. Cryo-EM structure and rRNA model of a translating eukaryotic 80S ribosome at 5.5-A resolution. *Proc. Natl. Acad. Sci. USA*. 107:19748–19753. http://dx.doi.org/10.1073/pnas.1009999107

Ben-Shem, A., L. Jenner, G. Yusupova, and M. Yusupov. 2010. Crystal structure of the eukaryotic ribosome. *Science*. 330:1203–1209. http://dx.doi.org/10.1126/science.1194294

Berisio, R., F. Schluenzen, J. Harms, A. Bashan, T. Auerbach, D. Baram, and A. Yonath. 2003. Structural insight into the role of the ribosomal tunnel in cellular regulation. *Nat. Struct. Biol.* 10:366–370. http://dx.doi.org/10.1038/nsb915

Cheng, Z., and R. Gilmore. 2006. Slow translocon gating causes cytosolic exposure of transmembrane and lumenal domains during membrane protein integration. *Nat. Struct. Mol. Biol.* 13:930–936. http://dx.doi.org/10.1038/nsmb1146

Cranney, M., R.B. Cundall, G.R. Jones, J.T. Richards, and E.W. Thomas. 1983. Fluorescence lifetime and quenching studies on some interesting diphenylhexatriene membrane probes. *Biochim. Biophys. Acta*. 735:418–425. http://dx.doi.org/10.1016/0005-2736(83)90156-6

Crowley, K.S., G.D. Reinhart, and A.E. Johnson. 1993. The signal sequence moves through a ribosomal tunnel into a noncytoplasmic aqueous environment at the ER membrane early in translocation. *Cell*. 73:1101–1115. http://dx.doi.org/10.1016/0092-8674(93)90640-C

Crowley, K.S., S. Liao, V.E. Worrell, G.D. Reinhart, and A.E. Johnson. 1994. Secretory proteins move through the endoplasmic reticulum membrane via an aqueous, gated pore. *Cell*. 78:461–471. http://dx.doi.org/10.1016/0092-8674(94)90424-3

Dell, V.A., D.L. Miller, and A.E. Johnson. 1990. Effects of nucleotide- and aurodox-induced changes in elongation factor Tu conformation upon its interactions with aminoacyl transfer RNA. A fluorescence study. *Biochemistry*. 29:1757–1763. http://dx.doi.org/10.1021/bi00459a014

Devaraneni, P., B.J. Conti, Y. Matsumura, Z. Yang, A.E. Johnson, and W.R. Skach. 2011. Stepwise insertion and inversion of a type II signal anchor sequence in the ribosome-Sec61 translocon complex. *Cell*. 146:134–147. http://dx.doi.org/10.1016/j.cell.2011.06.004

Do, H., D. Falcone, J. Lin, D.W. Andrews, and A.E. Johnson. 1996. The cotranslational integration of membrane proteins into the phospholipid bilayer is a multistep process. *Cell*. 85:369–378. http://dx.doi.org/10.1016/S0092-8674(00)81115-0

Erdmann, F., N. Schäuble, S. Lang, M. Jung, A. Honigmann, M. Ahmad, J. Dudek, J. Benedix, A. Harsman, A. Kopp, et al. 2011. Interaction of calmodulin with Sec61α limits Ca^{2+} leakage from the endoplasmic reticulum. *EMBO J.* 30:17–31. http://dx.doi.org/10.1038/emboj.2010.284

Erickson, A.H., and G. Blobel. 1983. Cell-free translation of messenger RNA in a wheat germ system. *Methods Enzymol.* 96:38–50. http://dx.doi.org/10.1016/S0076-6879(83)96007-X

Görlich, D., S. Prehn, E. Hartmann, K.-U. Kalies, and T.A. Rapoport. 1992. A mammalian homolog of SEC61p and SECYp is associated with ribosomes and nascent polypeptides during translocation. *Cell*. 71:489–503. http://dx.doi.org/10.1016/0092-8674(92)90517-G

Haigh, N.G., and A.E. Johnson. 2002. A new role for BiP: closing the aqueous translocon pore during protein integration in the ER membrane. *J. Cell Biol.* 156:261–270. http://dx.doi.org/10.1083/jcb.200110074

Hamman, B.D., J.-C. Chen, E.E. Johnson, and A.E. Johnson. 1997. The aqueous pore through the translocon has a diameter of 40-60 A during cotranslational protein translocation at the ER membrane. *Cell*. 89:535–544. http://dx.doi.org/10.1016/S0092-8674(00)80235-4

Hamman, B.D., L.M. Hendershot, and A.E. Johnson. 1998. BiP maintains the permeability barrier of the ER membrane by sealing the lumenal end of the translocon pore before and early in translocation. *Cell*. 92:747–758. http://dx.doi.org/10.1016/S0092-8674(00)81403-8

Hegde, R.S., and V.R. Lingappa. 1996. Sequence-specific alteration of the ribosome-membrane junction exposes nascent secretory proteins to the cytosol. *Cell*. 85:217–228. http://dx.doi.org/10.1016/S0092-8674(00)81098-3

Hegde, R.S., S. Voigt, T.A. Rapoport, and V.R. Lingappa. 1998. TRAM regulates the exposure of nascent secretory proteins to the cytosol during translocation into the endoplasmic reticulum. *Cell*. 92:621–631. http://dx.doi.org/10.1016/S0092-8674(00)81130-7

Johnson, A.E. 2005. Fluorescence approaches for determining protein conformations, interactions and mechanisms at membranes. *Traffic*. 6:1078–1092. http://dx.doi.org/10.1111/j.1600-0854.2005.00340.x

Johnson, A.E. 2009. The structural and functional coupling of two molecular machines, the ribosome and the translocon. *J. Cell Biol.* 185:765–767. http://dx.doi.org/10.1083/jcb.200902014

Johnson, A.E., and M.A. van Waes. 1999. The translocon: a dynamic gateway at the ER membrane. *Annu. Rev. Cell Dev. Biol.* 15:799–842. http://dx.doi.org/10.1146/annurev.cellbio.15.1.799

Johnson, A.E., W.R. Woodward, E. Herbert, and J.R. Menninger. 1976. Nepsilon-acetyllysine transfer ribonucleic acid: a biologically active analogue of aminoacyl transfer ribonucleic acids. *Biochemistry*. 15:569–575. http://dx.doi.org/10.1021/bi00648a018

Johnson, A.E., S. Liao, J. Lin, B.D. Hamman, H. Do, A. Cowie, and D.W. Andrews. 1995. The environment of nascent secretory and membrane proteins at the ER membrane during translocation and integration. *Cold Spring Harb. Symp. Quant. Biol.* 60:71–82.

Kida, Y., F. Morimoto, and M. Sakaguchi. 2007. Two translocating hydrophilic segments of a nascent chain span the ER membrane during multispanning protein topogenesis. *J. Cell Biol.* 179:1441–1452. http://dx.doi.org/10.1083/jcb.200707050

Liao, S., J. Lin, H. Do, and A.E. Johnson. 1997. Both lumenal and cytosolic gating of the aqueous ER translocon pore are regulated from inside the ribosome during membrane protein integration. *Cell*. 90:31–41. http://dx.doi.org/10.1016/S0092-8674(00)80311-6

Lin, P.-J., C.G. Jongsma, M.R. Pool, and A.E. Johnson. 2011. Polytopic membrane protein folding at L17 in the ribosome tunnel initiates cyclical changes at the translocon. *J. Cell Biol.* 195:55–70.

Lu, J., W.R. Kobertz, and C. Deutsch. 2007. Mapping the electrostatic potential within the ribosomal exit tunnel. *J. Mol. Biol.* 371:1378–1391. http://dx.doi.org/10.1016/j.jmb.2007.06.038

Ménétret, J.-F., A. Neuhof, D.G. Morgan, K. Plath, M. Radermacher, T.A. Rapoport, and C.W. Akey. 2000. The structure of ribosome-channel complexes engaged in protein translocation. *Mol. Cell*. 6:1219–1232. http://dx.doi.org/10.1016/S1097-2765(00)00118-0

Mothes, W., S.U. Heinrich, R. Graf, I. Nilsson, G. von Heijne, J. Brunner, and T.A. Rapoport. 1997. Molecular mechanism of membrane protein integration into the endoplasmic reticulum. *Cell*. 89:523–533. http://dx.doi.org/10.1016/S0092-8674(00)80234-2

Nissen, P., J. Hansen, N. Ban, P.B. Moore, and T.A. Steitz. 2000. The structural basis of ribosome activity in peptide bond synthesis. *Science*. 289:920–930. http://dx.doi.org/10.1126/science.289.5481.920

Pool, M.R. 2009. A trans-membrane segment inside the ribosome exit tunnel triggers RAMP4 recruitment to the Sec61p translocase. *J. Cell Biol.* 185:889–902. http://dx.doi.org/10.1083/jcb.200807066

Rapoport, T.A. 2007. Protein translocation across the eukaryotic endoplasmic reticulum and bacterial plasma membranes. *Nature*. 450:663–669. http://dx.doi.org/10.1038/nature06384

Reinhart, G.D., P. Marzola, D.M. Jameson, and E. Gratton. 1991. A method for on-line background subtraction in frequency domain fluorometry. *J. Fluoresc.* 1:153–162.

Sadlish, H., D. Pitonzo, A.E. Johnson, and W.R. Skach. 2005. Sequential triage of transmembrane segments by Sec61alpha during biogenesis of a native multispanning membrane protein. *Nat. Struct. Mol. Biol.* 12:870–878. http://dx.doi.org/10.1038/nsmb994

Saksena, S., M.D. Summers, J.K. Burks, A.E. Johnson, and S.C. Braunagel. 2006. Importin-alpha-16: a translocon associated protein that may facilitate sorting of integral membrane proteins to the nuclear envelope. *Nat. Struct. Mol. Biol.* 13:500–508. http://dx.doi.org/10.1038/nsmb1098

Shatursky, O., A.P. Heuck, L.A. Shepard, J. Rossjohn, M.W. Parker, A.E. Johnson, and R.K. Tweten. 1999. The mechanism of membrane insertion for a cholesterol-dependent cytolysin: a novel paradigm for pore-forming toxins. *Cell*. 99:293–299. http://dx.doi.org/10.1016/S0092-8674(00)81660-8

Shepard, L.A., A.P. Heuck, B.D. Hamman, J. Rossjohn, M.W. Parker, K.R. Ryan, A.E. Johnson, and R.K. Tweten. 1998. Identification of a membrane-spanning domain of the thiol-activated pore-forming toxin *Clostridium*

perfringens perfringolysin O: an α-helical to β-sheet transition identified by fluorescence spectroscopy. *Biochemistry*. 37:14563–14574. http://dx.doi.org/10.1021/bi981452f

Skach, W.R. 2009. Cellular mechanisms of membrane protein folding. *Nat. Struct. Mol. Biol.* 16:606–612. http://dx.doi.org/10.1038/nsmb.1600

Van den Berg, B., W.M.J. Clemons Jr., I. Collinson, Y. Modis, E. Hartmann, S.C. Harrison, and T.A. Rapoport. 2004. X-ray structure of a protein-conducting channel. *Nature*. 427:36–44. http://dx.doi.org/10.1038/nature02218

White, S.H., and W.C. Wimley. 1999. Membrane protein folding and stability: physical principles. *Annu. Rev. Biophys. Biomol. Struct.* 28:319–365. http://dx.doi.org/10.1146/annurev.biophys.28.1.319

Woolhead, C.A., P.J. McCormick, and A.E. Johnson. 2004. Nascent membrane and secretory proteins differ in FRET-detected folding far inside the ribosome and in their exposure to ribosomal proteins. *Cell*. 116:725–736. http://dx.doi.org/10.1016/S0092-8674(04)00169-2